Hypoxia in the Holocene Baltic Sea : Comparing modern versus past intervals using sedimentary trace metals

van Helmond, Niels A. G. M.

2018-08-20

van Helmond , N A G M , Jilbert , T & Slomp , C P 2018 , ' Hypoxia in the Holocene Baltic Sea : Comparing modern versus past intervals using sedimentary trace metals ' , Chemical Geology , vol. 493 , pp. 478-490 . https://doi.org/10.1016/j.chemgeo.2018.06.028

http://hdl.handle.net/10138/318417
https://doi.org/10.1016/j.chemgeo.2018.06.028

Hypoxia in the Holocene Baltic Sea: comparing modern versus past intervals using sedimentary trace metals

Niels A.G.M. van Helmond[a*], Tom Jilbert[a,b] and Caroline P. Slomp[a]

*Corresponding author: E-mail: n.vanhelmond@uu.nl

[a] Department of Earth Sciences, Faculty of Geosciences, Utrecht University. Princetonlaan 8a, 3584 CB Utrecht, Netherlands; n.vanhelmond@uu.nl (Niels A.G.M. van Helmond), c.p.slomp@uu.nl (Caroline P. Slomp)

[b] Ecosystems and Environment Research Program, Faculty of Biological and Environmental Sciences, University of Helsinki, Finland; tom.jilbert@helsinki.fi

Highlights (max. 5 ï max. 125 characters each)

- Holocene Baltic Sea sediments from hypoxic intervals are enriched in trace metals.
- The strongest enrichments in U are observed in recent sediments, indicating that modern oxygen depletion is most intense.
- Lower Mo in recent sediments compared with C_{org} and U, suggests depletion of the present-day water column Mo inventory.
- Enrichment of Re commences under mildly reducing conditions, but Re is not further enriched under more reducing conditions.
- Ni, Tl and Cu correlate with C_{org}, while Pb, Zn, As, Sb and Cd are all strongly influenced by anthropogenic pollution.

Abstract

Anthropogenic nutrient input has caused a rapid expansion of bottom water hypoxia in the Baltic Sea over the past century. Two earlier intervals of widespread hypoxia, coinciding with the Holocene Thermal Maximum (HTM_{HI}; 8-4 ka before present; BP) and the Medieval Climate Anomaly (MCA_{HI}; ~1200 ï750 years BP), have been identified from Baltic Sea sediments. Here we present sediment records from two sites in the Baltic Sea, and compare the trace metal (As, Ba, Cd, Cu, Mo, Ni, Pb, Re, Sb, Tl, U, V, Zn) enrichments during all three hypoxic intervals. Distinct differences are observed between the intervals and the various elements, highlighting the much stronger perturbation of trace metal cycles during the modern hypoxic interval. Both Mo and U show a strong correlation with C_{org} and very high absolute concentrations, indicative of frequently euxinic bottom waters during hypoxic intervals. During the modern hypoxic interval ($Modern_{HI}$) comparatively less Mo is sequestered relative to C_{org} than in earlier intervals. This suggests partial drawdown of the water column Mo inventory in the modern water column due to persistent euxinia and only partial replenishment of Mo through North Sea inflows. Molybdenum contents in modern sediments are likely also affected by the recent slowdown in input of Mo in association with deposition of Fe and Mn oxides. Strong enrichments of U in recent sediments confirm that the $Modern_{HI}$ is more intense than past intervals. These results suggest that U is a more reliable indicator for the intensity of bottom water deoxygenation in the Baltic Sea than Mo. Sedimentary Re enrichment commences under mildly reducing conditions, but this element is not further enriched under more reducing conditions. Enrichments of V are relatively minor for the MCA_{HI} and $Modern_{HI,}$ possibly due to strong reservoir effects on V in the water column, indicating that V is unreliable as an indicator for the intensity of bottom water

hypoxia in this setting. Furthermore, Ba profiles are strongly influenced by post-depositional remobilization throughout the Holocene. The strong relationship between C_{org} and Ni, Tl and particularly Cu suggests that these trace metals can be used to reconstruct the C_{org} flux into the sediments. Profiles of As, Sb and Cd and especially Pb and Zn are strongly influenced by anthropogenic pollution.

Keywords (max. 6)

Redox conditions, anthropogenic pollution, aqueous trace metal depletion, molybdenum, uranium

1. Introduction

Sedimentary trace metal records have widely been used as proxies for productivity and redox conditions in both modern and ancient aquatic systems (e.g. Calvert and Pedersen, 1993; Morford and Emerson, 1999; Tribovillard et al., 2006; Brumsack, 2006). Sedimentary trace metal concentrations are often low under a well-oxygenated water column (e.g. McLennan, 2001), while under low-oxygen conditions their concentrations are generally elevated due to the interplay of several related processes (e.g. Tribovillard et al., 2006).

Trace metals are closely associated with organic material in both the water column and in sediments (e.g. Pedersen and Calvert, 1990; Canfield, 1994; Tribovillard et al., 2006). Under well-ventilated conditions, only a fraction of the organic-bound trace metals in the water column reaches the sediment-water interface, due to efficient remineralization of organic matter in the water column. Under low-oxygen conditions, however, less organic material is remineralized leading to an

increase in the direct input of organic-bound metals to the sediments. Sediments are further enriched in trace metals under these conditions through uptake of trace metals by organic matter at the sediment-water interface.

A second key vector of trace metal transport to sediments is via Mn- and Fe(oxyhydr)oxides. Many trace metals are adsorbed onto oxide particles, which are highly mobile in seafloor environments where variable redox conditions lead to repeated cycles of dissolution and re-precipitation (e.g. Froelich et al., 1979; Shaw et al., 1990; Tribovillard et al., 2006). These processes can lead to the focusing of trace metals into defined areas of the seafloor (e.g. Lenz et al., 2015a). Although trace metal enrichment may occur under well-oxygenated conditions when metal-bearing Mn- and Fe-oxides are preserved in the sediments (e.g. Schaller et al., 2000), a more common route of enrichment is that metals are released during dissolution of oxides in the surface sediments, and subsequently sequestered in organic matter, sulfide minerals or other reduced authigenic phases (Morford and Emerson, 1999; Tribovillard et al., 2006).

A third pathway for trace metal enrichment is related to diffusive transport from seawater into sediments and subsequent sequestration in association with organic matter or authigenic minerals. Depending on the metal, enrichment may commence at various stages of bottom water oxygen depletion, i.e. the metal may be sequestered under hypoxic (dissolved oxygen concentrations < 2 mg/L), anoxic (no dissolved oxygen) or euxinic conditions (no dissolved oxygen and presence of free sulfide) (Crusius et al., 1996; Tribovillard et al., 2006; Olsson et al., 2017).

Two of the most studied and widely applied redox-sensitive trace metals, Mo and U, have many properties in common (see Algeo and Tribovillard, 2009 for an overview). One key difference between Mo and U is that the presence of free sulfide is a prerequisite for Mo enrichment in sediments. Sulfide is required to convert relatively unreactive seawater molybdate to particle reactive thiomolybdate (Helz et al., 1996). In contrast, authigenic U sequestration, primarily precipitated as uraninite (UO_2), already commences when Fe (III) is reduced to Fe (II) (Zheng et al., 2002), making U a potentially more sensitive recorder of minor changes in bottom water oxygen conditions. Another key difference is that water column Mo is actively scavenged by particle Mn- (and sometimes Fe) oxides, which may carry Mo to the sediment-water interface (e.g. Turekian, 1977; Adelson et al., 2001; Sulu-Gambari et al., 2017), whereas U is generally enriched via diffusion into sediments (e.g. Klinkhammer and Palmer, 1991). These differences in the sequestration of Mo and U can be used for detailed reconstructions of depositional conditions (Algeo and Tribovillard, 2009). In addition, the strong relation between C_{org} and Mo in euxinic environments can be used to identify basin reservoir effects, i.e. the depletion of an element in the water column of a stagnant basin through removal of that specific element to the sediment in excess of resupply by deepwater renewal. In this manner, aqueous Mo may become depleted, resulting in lower sedimentary Mo/C_{org} ratios (Algeo and Lyons, 2006).

Besides Mo and U, Re and V are the most studied and widely used redox-sensitive trace metals (e.g. Morford and Emerson, 1999; Morford et al., 2005). The low crustal abundance of Re results in relatively large, and therefore very distinctive, authigenic enrichments under reducing conditions (Koide et al., 1986; Crusius et al., 1996; Böning et al., 2004). Unlike for instance Mo, Re does not show an affinity for

126 Mn- and Fe-oxides and is sequestered in sediments under suboxic conditions after
127 diffusion across the sediment-water interface (e.g. Colodner et al., 1993; Morford et
128 al., 2012). Under well-oxygenated conditions V (in the form of vanadate oxyanions)
129 adsorbs onto Mn- and Fe-oxides (e.g. Wehrli and Stumm, 1989), but is also strongly
130 associated with organic matter (e.g. Beck et al., 2008), so both may be important
131 carriers of V to deeper waters or the sediment-water interface. Under moderately
132 reducing conditions, V(V) is reduced to V(IV), which is more surface reactive and
133 more easily complexes with (in)organic ligands (Emerson and Huested, 1991). This
134 may lead to enhanced sedimentary V sequestration, but the complexation of V(IV)
135 with dissolved organic matter may also allow it to remain in the aqueous phase (e.g.
136 O'Connor et al., 2015). In contrast with for instance Mo, V (e.g. Tribovillard et al., 2017
137 sequestration is not linked to the formation of authigenic sulfides (Algeo and
138 Maynard, 2004). However, under euxinic conditions V can be reduced to V(III),
139 which enables V sequestration through the precipitation of vanadium(hydr)oxide
140 (Wanty and Goldhaber, 1992).
141
142 A prime example, and perhaps the most widely used trace metal to reconstruct
143 marine primary productivity, is sedimentary Ba, which largely reflects biogenic barite
144 ($BaSO_4$), a remnant of decayed organic matter that is preserved in sediments (Bishop,
145 1988; Dymond et al., 1992; Schoepfer et al., 2015). The applicability of sedimentary
146 Ba as a (paleo)productivity proxy seems to be limited to open ocean settings, for
147 example, because a certain water depth (~1000 m) is needed in order to fully develop
148 the barite-productivity signal settings (Von Breymann et al., 1992; Plewa et al., 2012).
149 Its applicability is further complicated by remobilization of Ba under reducing
150 conditions (e.g. McManus et al., 1998; Henkel et al., 2012). Despite these

151 complications Ingri et al. (2014) showed that sedimentary Ba may represent primary
152 productivity in the Bothnian Bay during the last 5.5 kyr.
153
154 Furthermore, trace metal enrichments are also used to assess anthropogenic pollution
155 in (semi)modern sediments (e.g. Caccia et al., 2003; Ip et al., 2007). Many trace
156 metals have applications in agriculture and industry, e.g. in fertilizers, pesticides,
157 pigments and lubricants. These trace metals can be transported to the oceans by
158 fluvial and eolian pathways, where they are sequestered in sediments after adsorption
159 onto clay particles and (oxyhydr)oxides and complexation with organic compounds
160 (e.g. Nriagu and Pacyna, 1988; Windom et al., 1989; Liaghati et al., 2004).
161
162 The Baltic Sea is an ideal location to assess how changes in bottom water
163 oxygen, primary productivity and anthropogenic pollution are recorded by trace
164 metals in marine sediments. Its geographic configuration, i.e. landlocked with a
165 restricted connection to the open ocean (Fig. 1a), in combination with excessive
166 anthropogenic nutrient input (e.g. Gustafsson et al., 2012), has resulted in a tenfold
167 increase of the hypoxic area over the past century (Carstensen et al., 2014), creating
168 the world's largest human-induced dead zone (Diaz and Rosenberg, 2008). The
169 modern Baltic hypoxic interval (henceforth $Modern_{HI}$), was preceded by two previous
170 hypoxic intervals during the Holocene (Zillén et al., 2008). The first hypoxic interval
171 coincided with the Holocene Thermal Maximum (HTM_{HI}; ~8 and 4 ka before present
172 - BP). The second interval of widespread hypoxia in the Baltic Sea coincided with the
173 Medieval Climate Anomaly (MCA_{HI}; ~1200 – 750 years BP).
174

The laminated sediments marking the hypoxic intervals in the Baltic Sea are characterized by high organic carbon (C_{org}) and molybdenum (Mo) contents (Jilbert and Slomp, 2013a; Dijkstra et al., 2016; Hardisty et al., 2016; Papadomanolaki et al., 2018), indicative of free sulfide in bottom waters (Helz et al., 1996). Previous studies have drawn various conclusions about the environmental conditions during each of the hypoxic intervals. High-resolution records of Mo enrichment indicate that the development of the $Modern_{HI}$ was more rapid than the development of the MCA_{HI} and HTM_{HI}, while the maximum intensity of hypoxia was similar for all three events (Jilbert and Slomp, 2013a). In contrast, Hardisty et al. (2016) concluded, based on Mo isotopes, that reducing conditions during the MCA_{HI} and HTM_{HI} were probably more intense than during the $Modern_{HI}$. Focusing on the areal extent, rather than intensity, of hypoxia, Lenz et al. (2015a) concluded on the basis of sedimentary Fe records that the present-day hypoxic area is larger than that in the past.

Here we present a comprehensive analysis of trace metal enrichments during the three hypoxic intervals from two sites in the central Baltic Sea. By considering a large number of trace metals together, we are able to test multiple hypotheses about the mechanisms of trace metal enrichment, and the suitability of trace metals for paleoenvironmental reconstructions in this setting. Specifically, we investigate (1) the sensitivity of known redox-sensitive trace metal enrichments, i.e. Mo, U, Re and V, to variable redox conditions, (2) which trace metals may be reliable proxies for the organic carbon (C_{org}) flux into the sediments and (3) the effect of anthropogenic pollution on sedimentary trace metal records. We have generated complete discrete-sample records of 13 trace metals (As, Ba, Cd, Cu, Mo, Ni, Pb, Re, Sb, Tl, U, V, Zn), as well as major and minor sediment components (Al, Fe, S, C_{org}), for the entire

sediment column spanning the three hypoxic intervals and the intervening oxic periods, at two sites in the Baltic Sea (Fig. 1). Additionally, we present Laser Ablation – Inductively Coupled Plasma – Mass Spectrometry (LA-ICP-MS) line-scan Mo and U data for the three intervals at one of the two study sites. The LA-ICP-MS records allow an orders-of-magnitude increase in the depth resolution of the trace metal profiles, facilitating robust analysis of relative enrichments between Mo and U, and investigation of how the two elements respond to short-timescale changes in oxygen conditions.

2. Materials and methods

2.1 Study site

Sediment samples were retrieved from two different localities in the central part of the Baltic Sea during two research cruises with *R/V Aranda* in May-June 2009 and August 2013. Multicores (0-35 cm below seafloor; cmbsf) and gravity cores (~25-440 cmbsf) were collected from site F80 in the Fårö Deep (58.0000°N, 19.8968°E, 191 m water depth) and from site LL19 in the Northern Gotland Basin (58.8807°N, 20.3108°E, 169 m water depth; Fig. 1) in 2009. An additional short core (0-55 cmbsf) was taken at site F80 in 2013 with a GEMAX corer.

2.2 Processing of the sediment cores

The multicores and GEMAX core were sliced on board the ship under an oxygen-free atmosphere at in-situ bottom water temperature. The resolution of the sediment slices was 0.5 cm for 0-2 cmbsf, 1 cm for 2-10 cmbsf and 2 cm from 10 cmbsf until the bottom of the core. The GEMAX core for F80 retrieved in 2013 was sliced under the same conditions but with a resolution of 1 cm for the samples

analysed in this study (0-10 cmbsf). The gravity cores were stored at 4°C and sliced under an oxygen-free atmosphere in the laboratory at Utrecht University at a resolution of 1 cm. All sediment samples were freeze-dried and weighed before and after freeze-drying in order to determine the water content and to calculate porosity. The samples were subsequently powdered and homogenized using an agate mortar and pestle in an oxygen-free atmosphere.

2.3 Organic carbon content

Organic carbon content data (C_{org}) for the 2009 cores was generated and published by Jilbert and Slomp (2013a). For the 2013 GEMAX core 0.1-0.2 g of freeze-dried and powdered sediment sample was weighed in 15 ml centrifuge tubes and 7.5 ml of 1M HCl was added to dissolve carbonates. After four hours on a shaker the acid was removed through centrifugation and fresh 1M HCl was added after which the samples were left on a shaker overnight. The acid was then removed again after centrifugation and samples were washed twice with milliQ water, and dried at 60°C for 72 hours. The dried residues were then weighed again to determine the weight loss. Finally, the samples were powdered and homogenized and ~5 mg of each sample was weighed in a tinfoil cup. Total carbon analyses were performed using a Fisons Instruments NA 1500 NCS analyzer. Obtained results were normalized to in-house standards, acetanilide, atropine and nicotinamide. An internationally certified soil standard (IVA2) was measured after each 10 samples to determine the accuracy and precision of our analyses. The certified value for IVA2 is 0.732 wt.% C, our obtained mean value was 0.726 wt.% C with a standard deviation of 0.014 wt.% C. Finally, C_{org} was calculated upon correction for the weight loss due to the decalcification. An

249 average analytical uncertainty of 0.08 wt.% was calculated based on duplicate
250 analyses of sediment samples.
251
252 *2.4 Trace metal concentrations*
253 For the determination of sedimentary trace metal concentrations about 125 mg
254 of freeze-dried and powdered sediment sample was weighed in 30 ml Teflon vessels.
255 Subsequently 2.5 ml of mixed acid ($HClO_4$:HNO_3, 3:2) and 2.5 ml 40% HF were
256 added and the vessels were left overnight on a hotplate at 90°C. The following day the
257 lids of the vessels were removed and the extracts were heated to 140°C to evaporate
258 the acids. The remaining residues were then dissolved in 25 ml 4.5% HNO_3 and left
259 overnight on a hotplate at 90°C again. The dilution of the final solutions was
260 determined by weighing the vessels, after which the solutions were analysed by
261 Inductively Coupled Plasma-Optical Emission Spectrometry (ICP-OES; Al, Fe and S
262 published previously in Jilbert and Slomp, 2013a and Lenz et al., 2015a) and by
263 Inductively Coupled Plasma-Mass Spectometry (ICP-MS; As, Cd, Cu, Mo, Ni, Pb,
264 Re, Sb, Tl, U, V and Zn). For the latter analyses, we used an XSeries II ICP-MS
265 (Thermo Fisher Scientific) equipped with a Peltier cooled, low-volume conical spray
266 chamber fitted with a micro nebulizer, a micro pump and a FAST system on the
267 autosampler (SC-4 DX; Elemental Scientific), to enhance stability, enable fast
268 washout and minimum cross contamination and optimize sample throughput. The
269 accuracy (recovery) was generally between 95 and 105% for all reported elements
270 based on in-house standards. The average analytical uncertainty based on duplicates,
271 in-house standards and laboratory reference material (ISE-921) was 2% for As, 1%
272 for Cd, 2% for Cu, 1% for Mo, 2% for Ni, 2% for Pb, 8% for Re, 2% for Sb, 4% for
273 Tl, 2% for U, 2% for V and 2% for Zn.

274

275 *2.5 Resin Embedding and LA-ICP-MS*

276 Sections of the sediment cores from F80 (2009 gravity core and 2013
277 GEMAX core) were prepared for LA-ICP-MS analysis by resin embedding. From the
278 gravity core, U-channels of sediment (20 x 2 x 1 cm) were sampled horizontally from
279 the open core surface as described in Jilbert et al. (2008) and transferred immediately
280 to an N_2-filled glovebox. A total of 180 cm of sediment, including the laminated
281 intervals corresponding to the MCA_{HI} and HTM_{HI}, were sampled in this way. From
282 the GEMAX core, a vertical column of miniature sub-cores of sediment (8 sub-cores
283 in total, each 1 cm diameter, 7 cm length) was taken as described in Jilbert and Slomp
284 (2013a). The entire sub-coring operation was performed in a N_2-filled glove bag and
285 the sub-cores were transferred to an N_2-filled glovebox. All U-channels and sub-cores
286 were then dehydrated with argon-purged acetone, fixed in Spurr ô epoxy resin, and
287 sliced to reveal the interior surface using a water-cooled rock saw. The interior
288 surfaces were polished prior to subsequent analysis.

289 Resin-embedded sediment blocks were mounted in the ablation chamber of the
290 LA-ICP-MS instrument at Utrecht University. The ablation chamber sits on a mobile
291 stage. Line scan profiles were generated by focusing a pulsed argon-fluoride excimer
292 laser beam (120 µm spot size, 193 nm wavelength, 10 Hz repetition rate, 8 J cm^{-2}
293 energy density) onto the moving sample surface and ablating material into a high
294 mass-resolution ICP-MS (Thermo Element 2) via a He-Ar carrier gas. During line
295 scans the stage velocity was optimized to 0.0275 mm s^{-1} for high spatial resolution
296 measurements (Hennekam et al., 2015). Count rates of the isotopes ^{27}Al, ^{98}Mo and
297 ^{238}U, among a range of other elements, were determined continuously at a
298 measurement frequency of approximately 1 Hz.

The resin embedding procedure results in varying degrees of sediment compaction, such that the length of each line scan is less than that of the original U-channel or sub-core. To correct for compaction effects, the data from each LA-ICP-MS line scan was linearly re-scaled to the initial length of the sub-core. Subsequently, line scan data were fine-tuned by alignment to ICP-OES or ICP-MS data of discrete samples from the corresponding interval.

Raw LA-ICP-MS count data were converted to elemental compositional ratios via the two-step linear calibration procedure described in Jilbert and Slomp (2013a). Briefly, count rates of each element in the line-scan data were converted to preliminary concentrations using one-point sensitivity factors (counts/ppm) determined from a glass standard (NIST 610) at equivalent measurement settings. Preliminary concentrations of ^{98}Mo and ^{238}U were then normalized to ^{27}Al to correct for variable ablation yield during line scanning. The resulting ratios, corrected for natural isotopic abundances of each element, were further corrected using a linear regression against Mo/Al and U/Al concentration ratios of the equivalent sediment interval determined by discrete sample ICP-OES or ICP-MS analysis. This second step corrects for any offset between the sensitivity factors of the elements in the sediment sample relative to the standard glass.

2.6 Sediment chronologies

Age-depth models for the sediment cores used in this study were previously generated by Jilbert and Slomp (2013a) and Lenz et al. (2015a). For the present study we choose to show our data against depth instead of time. We have, however, included the dates, following Lenz et al. (2015a), in the supplementary data file. We follow Jilbert and Slomp (2013a) concerning the position of the $Modern_{HI}$, MCA_{HI}

and the HTM_{HI}. For the purposes of this study we do not discern different sub-events within the MCA_{HI} and HTM_{HI}.

3. Results

3.1 Trace metals in the Fårö Deep (site F80) and Northern Gotland Basin (site LL19)

The hypoxic intervals in the Fårö Deep are characterized by strong enrichments in sedimentary C_{org} (Fig. 2a). Maximum values are similar (~10 wt. %; Table 1) for the three hypoxic events when the top sediments consisting of fresh, non-degraded organic material, the so-called "fluff layer", are left out of consideration. Both Mo and U are also strongly enriched in the sediments of all three hypoxic intervals (Fig. 2a; Table 1). Maximum values for Mo (>300 ppm) are recorded during the HTM_{HI}. Background Mo concentrations, i.e. in the intervening oxic intervals, are 25 ppm on average (Table 1). Uranium concentrations progressively increase from the HTM_{HI} to the $Modern_{HI}$, hence the present-day U concentration is the highest in the record. In contrast with C_{org}, Mo and U, Re shows rather constant concentrations throughout the studied sediment sequence, without significant enrichments during the hypoxic intervals (Fig. 2a; Table 1). Both V and Ba are strongly enriched during the HTM_{HI}, but not during other intervals, in particular the $Modern_{HI}$.

The profiles of C_{org} and trace metals for the Northern Gotland Basin site LL19 (Fig. 2b) largely resemble those for the Fårö Deep (Fig. 2a). Maximum C_{org} values for the three hypoxic intervals are slightly lower than in the Fårö Deep, i.e. around 8 wt. % (Fig. 2b; Table 2). Maximum values for Mo are recorded during the MCA_{HI} and HTM_{HI}, with somewhat lower maximum values during the $Modern_{HI}$ (Fig. 2b). However, background Mo concentrations in the intervening oxic intervals (~6 ppm)

are much lower than in the Fårö Deep (Tables 1 and 2). Absolute U concentrations are also lower in the sediments of the Northern Gotland Basin, but the trend in U concentrations is the same as for the Fårö Deep, i.e. progressively increasing in the order HTM_{HI} iMCA_{HI} i$Modern_{HI}$. In contrast with the Fårö Deep, distinct enrichments in Re are observed during all three hypoxic intervals in the Northern Gotland Basin (Fig. 2b). Moreover, background Re concentrations in the intervening oxic intervals (10 ppb) are generally lower than in the Fårö Deep. Again, both V and Ba are strongly enriched during the HTM_{HI}, but strong enrichments are absent from the other intervals.

The other trace metals all show their strongest enrichments coinciding with the onset of the $Modern_{HI}$ (Fig. 3a). Significant enrichment in Zn is entirely confined to the $Modern_{HI}$, while for Pb there is also a small enrichment towards the end of the MCA_{HI}, followed by a rapid drop and a gradual increase towards the $Modern_{HI}$ (Fig. 3a). For Sb and As we observe both a strong $Modern_{HI}$-related enrichment and moderate enrichments during both the MCA_{HI} and HTM_{HI}, which generally follow the profiles of S and Fe (Fig. 3a). Enrichments in Cd, Ni, Tl and Cu are more similar to those of C_{org} and Mo. Even the smaller variations in C_{org} and Mo, e.g. the maximum around 410 cmbsf (Fig. 3a), are clearly expressed, and the absolute magnitude of the enrichments in Ni, Tl and Cu is rather similar for all three of the hypoxic events.

As for the Fårö Deep, significant enrichment in Zn in the Northern Gotland Basin is confined to the $Modern_{HI}$, while for Pb there is also a small enrichment visible towards the end of the MCA_{HI}. For Sb, As, Cd, Ni Tl, and Cu, there are, besides the strong $Modern_{HI}$-related enrichment, clear enrichments visible during both

the MCA_{HI} and HTM_{HI} (Fig. 3b). The magnitude of the enrichments in Ni, Tl and Cu is again similar for the three different hypoxic intervals, while for Sb, As and Cd, the enrichment during the $Modern_{HI}$ is much larger than the enrichments during the MCA_{HI} and HTM_{HI} (Fig. 3b).

3.2 High-resolution molybdenum and uranium records

Trends in the high-resolution Mo and U LA-ICP-MS data for each of the hypoxic intervals in the Fårö Deep (Fig. 4) are in good agreement with the results for the discrete samples (Fig. 2a). However, the LA-ICP-MS data reveal significantly more internal variability within these intervals, and rapid changes in enrichment as previously demonstrated by Jilbert and Slomp (2013a) for shorter sections of the Holocene record. Moreover, the LA-ICP-MS data clearly show that U enrichment increases gradually at the onset of centennial-scale ôhypoxic eventsô with hypoxic intervals (zoom sections labeled ôonsetô in enrichments increase rapidly beyond a certain point in the development of each event.

The contrast between relative Mo and U enrichments in each hypoxic interval is further illustrated by the LA-ICP-MS data. Although both elements are clearly enriched in all intervals, the Mo/U ratio differs markedly between HTM_{HI}, MCA_{HI} and $Modern_{HI}$. In hypoxic events within HTM_{HI}, Mo/U oscillates around 10, while in MCA_{HI} the average value is close to 5, and for $Modern_{HI}$ the average value is close to 3.5 (Fig. 4).

4. Discussion

399 *4.1 Molybdenum and uranium as proxies of bottom water redox conditions*

400 The extremely high concentrations of Mo during the three hypoxic intervals
401 can only be explained by persistent euxinic conditions at these times (e.g. Scott and
402 Lyons, 2012), as concluded by previous studies of Baltic Sea sediments (Jilbert and
403 Slomp, 2013a; Dijkstra et al., 2016). The similar maximum values of C_{org} and Mo for
404 the three hypoxic intervals have previously been interpreted to indicate that the
405 intensity of hypoxia during each interval was similar (Jilbert and Slomp, 2013a).
406 However, the increase in U concentrations from the HTM_{HI} to the $Modern_{HI}$ observed
407 in our new data causes us to reassess this conclusion. Taken alone, the U records
408 suggest that the intensity of the hypoxic intervals has in fact increased towards the
409 present day. This would imply that increased anthropogenic nutrient inputs to the
410 Baltic during the 20th century (e.g. Gustafsson et al., 2012; Carstensen et al., 2014)
411 have led to a perturbation of trace metal cycling that exceeds the natural variability
412 observed in earlier hypoxic intervals.
413
414 The average background Mo concentration of 25 ppm in the Fårö Deep
415 suggests that even outside the hypoxic intervals, bottom waters in this location may
416 have been intermittently euxinic (Scott and Lyons, 2012). The lower average
417 background Mo concentration in the Northern Gotland Basin (6 ppm), although
418 substantially above the crustal average (~1-2 ppm; McLennan, 2001), is significantly
419 below that of the Fårö Deep, suggesting that sulfide remained restricted to pore waters
420 (Scott and Lyons, 2012). This difference can be attributed to the greater water depth
421 of the Fårö Deep (191 m versus 169 m), making it naturally more susceptible to
422 deoxygenation. The relatively early onset of U enrichment compared to Mo during
423 short-timescale hypoxic events within the HTM_{HI}, MCA_{HI} and $Modern_{HI}$ in the Fårö

7KH VHTXHQFHV ZHUH QHDUO\ LGHQWLFDO WR HDFK RWKHU DQG GLYHUJHQFH EHWZHHQ WKHP 7KH PDJHGRVSKDHQVUHFHQVLRQDO\%DVV 6ORZ GLVWDQFH WR B.) sphaeropsis TXHQFH RI WR ƒ 6 ƒ (± FRPSDUHG WR D PXFK GHHSHU 0D± GLVWDQFH WR RWKHU VSHFLHV RI WKH VXEJHQXV 7KH WZR VSHFLHV LQGHHG RKDYH FHUWDLQ 3 MXYHQLOH PRUSKRORJLFDO VLPLODULW\ VHH 24&RPSDUHG %R YRXFKHU D PRUH H[WHQVLYH WDLQ DQG JHQH VDPSOLQJ VKRXOG UHYHDO DGGLWLRQDO 'LDJQRVLV $QWHURGRUVDO PDUJLQ RI ZLWK UDWKHU VKRUW DFXWH SRLQW GLUHFWHG URVWUXP UHDFKLQJ SRVWHULRU HGJH RI SHGXQFOH VHJPHQW ÀDQNHG E\ QHDU PDUJLQV QRW IRUPLQJ DQJOHV 7HOVRQ WLPHV DV ORQJ DV ODVW DEGRPLQDO ORQJ DV ZLGH DQWHULRUO\ DQG ± DV DQWHULRUO\ 7HOVRQ ODWHUDO P FHQWUDO SDUW ZLWK ± VSLQLIRUP VHUULHV VHWDH LQFUHDVLQJ LQ OHQJ WHUPLQDO VSLQLIRUP VHWDH ORQJHV ± WLPHV DV ORQJ DV VKRUWHU PH DERX UDWKHU ORQJ VSLQXOHV (\H PRGHUDWH LQ VL]H EURDG VOLJKWO SODWH ,, RI ¿J HDG ZLGWK FRQHD VKRUW QRW GRPLQDWLQJ RYHU H\HVWDON H\H ORQJ $QWHQQXODU SGXQFOH H[WHQGL VFDOH)LJ $ ' $QWHQQDO VFDOH)LJ ORQJ DV ZLGH LWV GLVWRODWHUDO VS VSLQXOHV DSLFDOO\ ZLWK RQO\ VOLJK DQJOH QRW H[FHHGLQJ EH\RQG GLVWH 0•OOHU 3HWU\DSKRY D ± ¿J +DUJUHDYHV /RZU\ 6WRGGDUW 6DZDPRWR Boreomysis spinifera& RLIPDQQ SODWH D±H SODWH ¿J I J : 0 7DWW)HUVDOO D VHJPHQWHG 3HUSRG SURSRGXV V DV ORQJ DV VHJPHQW 8URSRGDO H[R > 1 RBoreomysis spinifera + ROPTXLVW ± ¿J %LUVWHLQ 7FKLQGRQRYD ORQJHU DQG VOHQGHU VSLQLIRUP VHWDH LWV SUR @ UDPXV OHQJWK (QGRSRG)LJ / ZLW VSLQLIRUP VHWDH RU ZLWKRXW WKHP Type material 6\QW\SHV PDOH DQG IHPDOHV ,QGRQHVLD f 6 f Sibog aR OVW Q 1 % & 0$ Body length ± PP &586 (Material)HPDOH LOOXVWUDWHG &RPSDUHG WR 7DVPDQLDQ)QGHUV KDYH DQ\ XQLTXH FKDUDFWHUV LQ WKH J WR f 6 f (± P EH FOHDU\ f HVWDEOLVKHG DVB ZHOO ,W FROO %37 / (|KXJHU .)XS.UL\DQRYD (B.) brucei \ : 0 7DWWHHB (B.) California 2UPDQ ,1 B9 B %(6 $0 3 MXYHQLOH (B.) intermedia DQG (B.) sibogae LV QRW NQRZQ \HV LOOXVWUDWHG 1HZ 6RXWK :DOHV RB. (B.) sibogae DQG WKHLU WD[RQRPLF VWDV f (WR f 6 f (± 5HPDUNV (B.) California LW LV GLVWLQJXLVK FROO VDPH DV SUHYLRXV ,1 B9 B %(6 $0 WKH VPHZKDW VKRUWHU WHOVRQ FOHIW 3 MXYHQLOH VDPH DV SUHYLRXV $0 3 WHOVRQ QHQJWK %DON DQG WKH GLVW 24 YRXFKHU % VXEDGXOW PDOH WUDQVLWLRQDO %DVV 6WUDLW LURP f 6 MXYHQLOHV 1HZ 6RXWK :DOHV Ru %HUPDJXL SDUW RI WKH HQGRSRG VFDOH QRW SU f (WR f 6 f (± SURGXFHG (B.) California 0D\ FROO VDPH DV SUHYLRXV 1 B9 B %(6 $0 3 VXEDGXOW PDOH WHOVRQ Description of Australian specimens (adults) $QWHURGRUVD 6RXWK :DOHV &HQWUDO (DVWHUQ &RPPRQZHDOWK 0DULQH 5HVHUYH IURP f 6 f (WR f ± P -XQ FROO VDPH DV SUHYLRXV 9 B %(6 $0 3 MXYHQLOH +XQWHU &RPPRQZHDOWK 0DULQH IURP f 6 f (WR f ± P -XQ FROO VDPH DV SUHYLRXV ,1 B9 B %(6 $0 3 MXYHQLOH 7DVPDQLD %DV 6WUDLW IURP f 6 f (WR f ± P -XQ FROO VDPH DV SUHYLRXV ,1 B9 B %(6 $0 3 MXYHQLOHV 1HZ 6RXWK :DOHV &HQWUDO (DVWHUQ &RPPRQZHDOWK 0DULQH 5HVHUYH IURP f 6 f (± P WR

Boreomysis (Boreomysis) sibogae Hansen, 1910

) L J

Boreomysis sibogae + DQVHQ SODWH ,, D±H : 0 7DWWHUVDOO 1LHUVWUDV] %UHQGHU j %UDQGLV ²1RXYHO ²: 0 7DWWHUVDOO 2 6 7DWWHUVDOO ²2 6 7DWWHUVDOO ²+ROPTXLVW ± ²*RUGRQ ²%LUVWHLQ 7FKLQGRQRYD ± ²3LOODL ¿J DIWHU +DQVHQ 0DXFKOLQH 0XUDQR ²)HQWRQ ± ¿J ± DIWHU +DQVHQ SODWH ,, ¿J et al ²/DQFUDIW 0•OOHU ²3HWU\DSKRY D ± ¿J ²+DUJUHDYHV /RZU\ 6WRGGDUW ²6DZDPRWR

Boreomysis spinifera& RLIPDQQ SODWH D±H SODWH ¿J I J ²: 0 7DWW)HUVDOO D

> 1 RBoreomysis spinifera² + ROPTXLVW ± ¿J ²%LUVWHLQ 7FKLQGRQRYD @

Type material 6\QW\SHV PDOH DQG IHPDOHV ,QGRQHVLD f 6 f Sibog aR OVW Q 1 % & 0$

Material)HPDOH LOOXVWUDWHG &RPSDUHG WR 7DVPDQLDQ)QGHUV KDYH DQ\ XQLTXH FKDUDFWHUV LQ WKH J WR f 6 f (± P EH FOHDU\ f HVWDEOLVKHG DVB ZHOO ,W FROO %37 / (|KXJHU .)XS.UL\DQRYD (B.) brucei \ : 0 7DWWHHB (B.) California 2UPDQ ,1 B9 B %(6 $0 3 MXYHQLOH (B.) intermedia DQG (B.) sibogae LV QRW NQRZQ \HV LOOXVWUDWHG 1HZ 6RXWK :DOHV RB. (B.) sibogae DQG WKHLU WD[RQRPLF VWDV f (WR f 6 f (± 5HPDUNV (B.) California LW LV GLVWLQJXLVK FROO VDPH DV SUHYLRXV ,1 B9 B %(6 $0 WKH VPHZKDW VKRUWHU WHOVRQ FOHIW 3 MXYHQLOH VDPH DV SUHYLRXV $0 3 WHOVRQ QHQJWK %DON DQG WKH GLVW 24 YRXFKHU % VXEDGXOW PDOH WUDQVLWLRQDO %DVV 6WUDLW LURP f 6 MXYHQLOHV 1HZ 6RXWK :DOHV Ru %HUPDJXL SDUW RI WKH HQGRSRG VFDOH QRW SU f (WR f 6 f (± SURGXFHG (B.) California 0D\ FROO VDPH DV SUHYLRXV 1 B9 B %(6 $0 3 VXEDGXOW PDOH WHOVRQ Description of Australian specimens (adults) $QWHURGRUVD 6RXWK :DOHV &HQWUDO (DVWHUQ &RPPRQZHDOWK 0DULQH 5HVHUYH IURP f 6 f (WR f ± P -XQ FROO VDPH DV SUHYLRXV 9 B %(6 $0 3 MXYHQLOH +XQWHU &RPPRQZHDOWK 0DULQH IURP f 6 f (WR f ± P -XQ FROO VDPH DV SUHYLRXV ,1 B9 B %(6 $0 3 MXYHQLOH 7DVPDQLD %DV 6WUDLW IURP f 6 f (WR f ± P -XQ FROO VDPH DV SUHYLRXV ,1 B9 B %(6 $0 3 MXYHQLOHV 1HZ 6RXWK :DOHV &HQWUDO (DVWHUQ &RPPRQZHDOWK 0DULQH 5HVHUYH IURP f 6 f (± P WR

Figure 4 Boreomysis (Boreomysis) sibogae, D–G, I–K) I H P D O H P P 7 D V P D Q L \ X S E D G X O W P D O H 1 H Z 6 $ 0 3 (C) M X Y H Q L O H 1 H Z 6 R X W K H D V W H D G X O W P D O H 1 H Z 6 R X W K H D G H D S W H U D U R V W U X P D Q G C H U R V W U D X P H D Q G H K H D G E A S R V W H U R U P D U J L Q F R S R E W H U Q P D R I D E G R P H Q D Q G W H O V R Q O D W H U D Q G S W O W H R U P Y S D W H R Q W K R Q X V H O H Q G R S R G (K) Y H Q R S U R G O H [R S R G P R V W R I V H W D H Q R W V K R Z Q V / P S H U R S R G

Boreomysis (Boreomysis) sphaerops L., 1964

)LJV

Boreomysis sphaerops L.
± ¿JV ± ²0•OOHU
Boreomysis spinifera² %LUVWHLQ 7FKLQGRQ\D
¿J

Type specimens ,L EDVHG KLV GHVFULSWLRQ D
ODUJH VHULHV RI VSHFLPHQV IUP ZKLFK D PP PDOH ZDV
GHVLJQDWHG DV ³W\SH´ DQG VKRXOG SURHDEO\ EH WUHDWHG DV WKH
KRORW\SH -DSDQ 6KL]XRND 3UHIHFWXUH 6DJDP\ %D\ DQ LVOHW
QHDU $MLUR PLOHV >FD NP@ ZHVW RI ±DVKLPD ±PWLFXODUO
$SU KDXO 1R (YHUWLFDO QHW •V FROOHFWLRQ 1R
E DQG D PP IHPDOH ZDV GHVLJQDWHG DV ³DQRWKHU
VDPH ORFDOLW\ 0DU KDXO 1R 6WDWXV XQNQRZQ

Type locality -DSDQ 6KL]XRND 3UHIHFWXUH 6DJDP L %D\ DQG
LVOHW QHDU $MLUR DERXW NP 1RUWKHDVW RI ±DVKLPD

Material)HPDOH VXEDGXOW PP %\URQ %D\ IURP f 6 f
f (± P -XQ 7UDZOHU &59
%37 / (+XJKHVH(U . . .XSUL\DQRYDSH GXQH VHJPHQW
9 B %(6 $0 3 PDOH
GDPDJHG PP MXYHQLOH 1HZ 6RXWK :DOHV
(DVWHUQ &RPPRQZHDOWK 0DULQHV 3HUPHUQW IURP WK
f (WR f 6 f (±
-XQ FROO VDPH DV SUHYLRXV
3 PDOH VXEDGXOW VDPH DV
*HQ%DQN 24 YRXFKHU %

Body length PP LPPDWXUH LQ $XVWU
± PP 1RUWK :HVW 3DFL¿F

Comparison Boreomysis (B.) sphaerops L. V UDWKHU VL
WR (B.) obtusata * 2 6DUV IURP ZK
GLVWLQJXLVKHG E\ WKH SUHVHQFH
WKH WHOVRQBF(B.)obtusata DERVHQW
WHUPLQDO VSLQLIRUP VHWDH RI WKH
WKH ÀDQNLQJ RQHV DE(B.)obtusata
WKH UDWKHU ELJ H\HV ZKLFK ZKH
WRXFKLQJ HDFK RWKHU E\ ODWHUDO
VSHFLPHQV EH\RQG WKH KHDG(B.)VLGHV
obtusata DQG E\ WKH VKDSH RI WKH H\H
GLVWLQJXLVKHG RPPDOH ZRV
VWDON DERXW WKH GRU
LV DVLPLODUL\ LQ WKH VKDSH RI
ZLHDVW RI ±DVKLPD ±PWLFXODUO
R WKH O DWHUDO(B.)Sphaeropsobtusata WKH UHV
VKRUW URVWUDO(B.)inopinata VS QRY DQG WKH VOLJKWO
WHOVRQ FOHIW KDYLQJ WKH(B.)QWHUL
inopinata VS QRY DQG WKH VOLJKWO\
inopinata VS RI ±DVKLPD

Distribution Australian specimens $QWHURGRUVDO
R(FDUDSDFH ZLWK UDWKHU VKRUW
RXWHU VHJPHQW ÀDQNHG E\ VP
OXDEVHGXOW\ ZLWKRXW PLQXWH FRQFD
WHUPLQDO VSLQHV 1HZ 6RXWK :DOHV
IURP WK ƒDSLFDOO\ SRLQW
WR ± WLPHV DV ORQJ DV OD
DQWHULRUO\ 7HOVRQ ODWHUDO PDU

Figure 5 Boreomysis (Boreomysis) sphaeroma (A–F, H–N) V X E D G X O W I H P D O H 1 H Z 6 R X W K :DOHV $XVWUDOLDQ 0XVHXP 9RO
6 R X W K :DOHV $XVWUDOLDQ 0XVHXP 9RO
XURSRGV VHWDH (QRSVRVWHUQLWH GRUDOO DQWHQQDH DQG SHUHRSRGV
PLVVLQJ GLVWDO SDUW HIODJHOODQW DQWHQQDH DQG SHUHRSRGV
GRUVDSDUV FHQWUDOL]HG RPDWLGLXP SRVWHULRU 6FDOHV PP $±.

Figure 6 Boreomysis (Boreomysis) sphaeropsX E D G X O W I H P D O H 1 H Z 6 R X W K D : D O H V S H G 3 H Q G R S R G
(B) P D [L O O L S H G (C) S D U W R S R G U H Q G R S R G D Q W H U L R U 6 F D O H V P P


Variation
Distribution and habitat
Molecular characters
Remarks
Etymology
Diagnosis
Description
Type locality
Material examined

Figure 7 Boreomysis (Petryashovia) urospina, adult male, holotype (AM W.29999). A, dorsal view; B, lateral view; C, ventral view; D, frontal view; E, antennule; F, antenna; G, mandible; H, maxillule; I, maxilla; J, maxilliped; K, pereopod 1; L, pereopod 2; M, pereopod 3; N, pereopod 4; O, pereopod 5; P, pleopod 1; Q, pleopod 2; R, pleopod 3; S, pleopod 4; T, pleopod 5; U, uropod; V, telson. Scales: A–C, 5 mm; D, 2 mm; E–V, 1 mm.

Body length RI IHPDOHV ± PP RI PDQ\ KDV D PLQXWH IHDWXUHV IRU WKH VXEJHQXV DQG KDV D PLQXWH FRQFDYLW\ RQ LWV ODWHUDO HYHQ DPRQJ RWKHU Boreomysis VSHFLHV XURSRGDO H[RSRG LV UDWKHU ZLGH WR WHQ WLPHV DV ORQJ DV ZLGH EHDULQJ WKUHH VSLQLIRUP VHWDH RQ WKH UDPXV DQG RQH RU WZR LQ RWKHU VSHFLHV RWKHU VHWDH RQ WKH UDPXV HQGRSRG LV ZLWK WKUHH RU ¿YH PHGLDO VSLQLIRUP VHWDH WZR LQ RWKHU VSHFLHV Boreomysis VHWDH RQ ODWH DQG WKH XURSRGDO FRQWUDVW ZLWK HQGRSRG LV ZLWK WKUHH RU ¿YH PHGLDO VSLQLIRUP VHWDH WZR LQ RWKHU VSHFLHV

Comparison Boreomysis (P.) urospina VS QRY KDV XQLTXH IHDWXUHV IRU WKH VXEJHQXV KDV D PLQXWH FRQFDYLW\ RQ LWV ODWHUDO HYHQ DPRQJ RWKHU Boreomysis VSHFLHV XURSRGDO H[RSRG LV UDWKHU ZLGH WR WHQ WLPHV DV ORQJ DV ZLGH EHDULQJ WKUHH VSLQLIRUP VHWDH RQ WKH UDPXV DQG RQH RU WZR LQ RWKHU VSHFLHV RWKHU VHWDH RQ WKH UDPXV HQGRSRG LV ZLWK WKUHH RU ¿YH PHGLDO VSLQLIRUP VHWDH WZR LQ RWKHU VSHFLHV Boreomysis VHWDH RQ ODWH DQG WKH XURSRGDO FRQWUDVW ZLWK HQGRSRG LV ZLWK WKUHH RU ¿YH PHGLDO VSLQLIRUP VHWDH WZR LQ RWKHU VSHFLHV Boreomysis VHWDH RQ OHQJWK DQG WKH XURSRGDO FRQWUDVW ZLWK HQGRSRG LV ZLWK WKUHH RU ¿YH PHGLDO VSLQLIRUP VHWDH WZR LQ RWKHU VSHFLHV B. (P.) megalops PRVW VLPLODU WR GLuHULQJ IURP LW LQ DGGLWLRQ IURP FKDUDFWHUV E\ WKH ORQJHU DQWHQQXOH DQG WKH WHOVRQ KDYLQJ RQO\ WZR SDLUV RI ODWHUDO VSLQHV DQG WKH WHOVRQ KDYLQJ RQO\ WZR SDLUV RI ODWHUDO VSLQHV PDOH SOHRSRGV ERWK B. (P.) megalops DQG WKH WHOVRQ KDYLQJ ODUJHU VHWDH IRU B. (P.) megalops WZR LQ

Description of holotype male $QWHURGRUVDO FHSKDORJDVWULF UJLQ DSLFDO VSLQLIRUP FDUDSDFH DQJXODU DSLFDO\ DW HDFK VLGH DQWHURODWHUDO SRLQWHG 3RVWHURODWHUDO PDUJLQ DSLFDO\ EOXQW RU URXQGHG DQJXODU DSLFDO\ ORQJ DV ODVW DEGRPLQDO VHJPHQW ZLWK VKRUW VSLQH DW HDFK VLGH DQWHURODWHUDO DQJOH DQG ORQJ SRVWHURODWHUDO VSLQH

Figure 8 Boreomysis (Petryashovia) urospina VS (A, C, E–H, J, K) KRORW\SH PDOH (B, D, I) $OO3OR W\SH IHP
PP $03 (A, B) KHDG (G) RKHDG (D) DKHDG OF DUDSDFH QER VSRVKRZLQL RO DSDHUWDR I D
WHOVRQ DQG XURSRGV VHWDH DQG VSH QSLRRWWHVLHRWDHDFUJVQORIQDEGRVKHQQDQ
OHIW VLG (E) SYRQWUDU PDUJLQ (H) WEEGSRQWHOLDVHDQWRQDHQ (J) DQWHQQD (K) XURSRGDO
HQGRSRG YHQWUDO 6FDOHV PP

Figure 9 Boreomysis (Petryashovia) urospina VS QRY KRORW\SH PDOH(A) ODFFU XSP0(B)HPQDWQGLE XODU SDOS SRCVWHJKWUPQGDEOHIWHPQDWQGLE(C)HPD[LOHQDWUDFSDVLHOOLRU(G)DPQDWHOLSHG DQW(H)UGLRFW\ODU FODZ(I)RPHGL[DOOVLSWHG RI PD[(J)DSLHGLSEDKPHQDWLRU UDWVHWD RI PD[LOO(K) SHGLDOD FWWWDXVRI PD[LQ(L)SHGLDOD SRIPD[LOOHRSRGSRIQ(M)SHGLDOD FWDUDUXVRI(N)HPHUGLDO VHWDH RI(PS)HPHUHGLSRGVHWDHRVQHSHDRSRGD FWF\DUDSUXV(R)VHWDQLVSHUH ODWHUDO 6FDOHV PP $±* - 0 1 5 + , . / 4 2 3

Neobirsteiniamysis
Hendrickx et Tchindonova, 2020

Type species: *Petalophthalmus inermis* L O O H P R H V 6 X K P

Diagnosis 7 H O V R Q U D W K H U E U R D G L Q W K H F R Q F D Y L W \

Description of female $ Q W H Q Q X O D U S H G X Q F O H V H J P H Q W

Colour 5 H G) L J

Distribution and habitat 5 H F R U G H G R Q O \ I U R P W K H V R X W K H U Q

Molecular characters 7 Z R Q H D U O \ L G H Q W L F D O V H T X H Q F H V R I

Habitat % D W K \ D O D E \ V V D O H S W K ±

Remarks 6 S H F L P H Q V U L Q W K L V J H Q X V Z H U H

Petalophthalmus: L O O H P R H V 6 X K P : L O O H P R

Neobirsteiniamysis inermis
(Willemoes-Suhm, 1874)

Petalophthalmus inermis: L O O H P R H V 6 X K P [Y [L

Petalophthalmus armiger: 7 L F K L H O R R R Y 6 X K P [L Y

Figure 11 Neobirsteiniamysis inermis I H P D O H P P *U H D W $ X V W U D O L D Q %L J K W $0 3 6
* +R O P H V Z L W K S H U P L V V L R Q

Figure 12 Neobirsteiniamysis inermis(A–F) I H P D O H P P * U H D W $ X V W U (C) L X E D % L J K W I H P D O H % D V $ 0 3 (A) K H D G (B) R D Q W H Q Q X O D U S (C) G X H Q F D H S Y H Q W H U D Q O R Q R X W H U À D J H O O X P R I (D) D Q W H Q Q X O D U S E H G U R F L P H O G R V W R H D S Q W H L P D G S R U W R G D Q W H Q Q D O H V E W O E O P P $ % ' ± * &

Figure 13 Neobirsteiniamysis inermis(A–D, F) I H P D O H P P * U H D W $ X V W U(E)O\LXDEQD%LDKWIHPDO3H %
$0 3 (A) K H D G (B)D SVRHVUDHU L R U S D U(C)\ SRR VEVRHGU L RGR UPVDDUJ L Q(D) ISRE\GVRHRUHLQR U OFDWU
D E G R P H Q (E)Y HVQHMOFHDIDKQ R S R G V Y H Q W U D O 6 F D O H P P

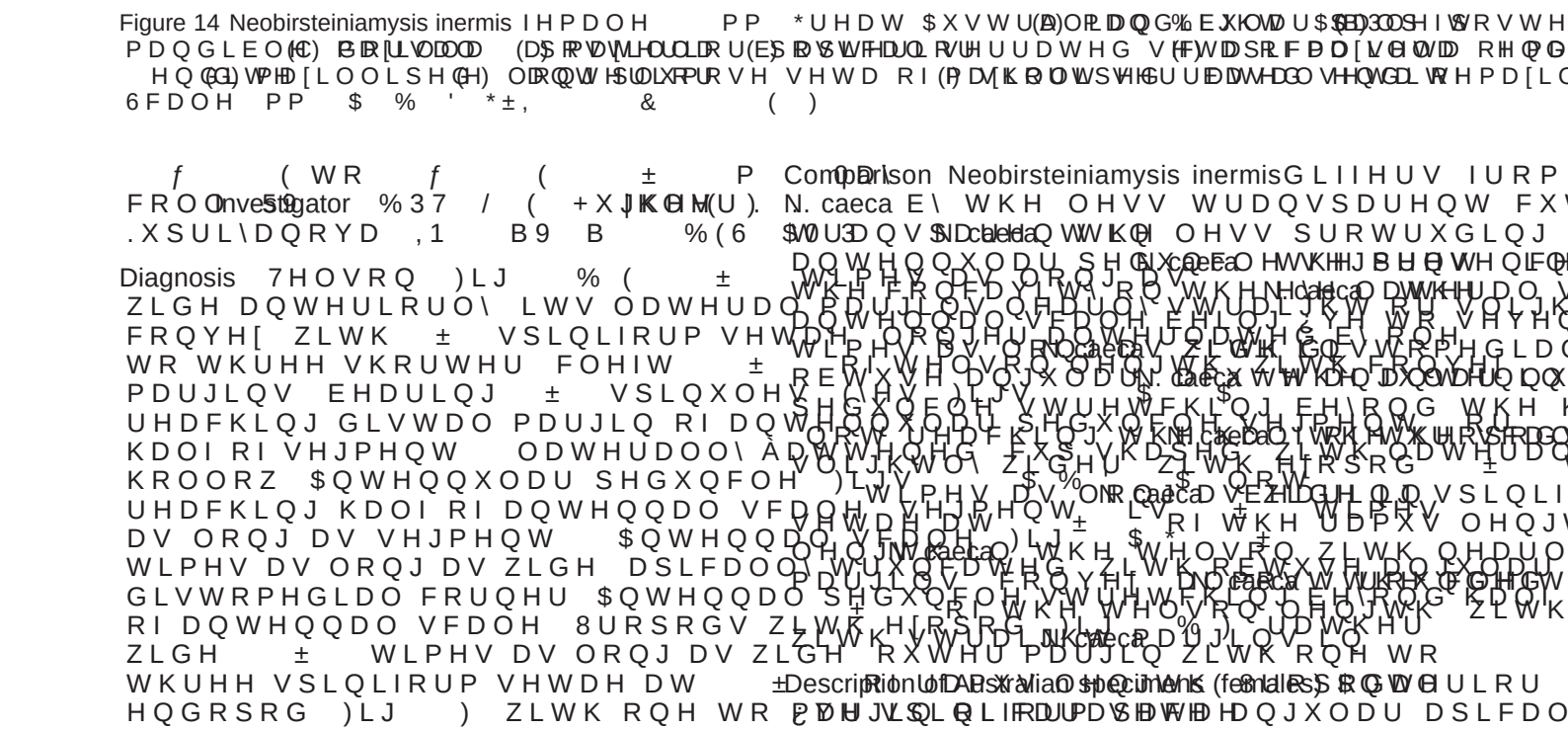

Figure 14 Neobirsteiniamysis inermis, holotype, AM P.

Comparison of N. caeca by the lesser antennal peduncle segment, and Diagnosis by the antennular rostral margin, and the antennal scale.


Body length
Coloration

Figure 16 5HFRUGV RI WKH VSHFLHV RI WKH VXEIDPLO\ %RUHRP\VLQDH LQ $XVWUDOO

± ƒ& WR ± ƒ& 3HWU\DVKRY VSHFLPHEQXW RHQJHUBDSyphoG%HVWUKLEVHG, D
HXU\WKHUPDO VSHFLHV FDSDEOHGRI QORWLQJL QG WKSURDQVHREHWZHHQ¶V
± ƒ& DQG ƒ& 3HWU\DVKRY D1RUQWKHUQ 1DRUWKSXWCKHQWQLFHPLVSHUV
IRXQG DW WHPSHUDWXUH RI ± ƒ& ,WRK± V PDWRYUHZRUN WDEOHWVRQ GH
* 2 6DUV D %UDWWHJDUG VSHHDLDHYGis +DQVHQ WKH IURP WKH (D
1RUWK 3DFL¿F DW WHPSHUDWXUHRI SHGƒ&WR ƒ&RREYDEUiDPiGRWWDVVRF
DQG VDQG\ ERWWRP RFFDVLRQDOO\ HSUDHWRQF+DRIVHRFNV DQGEVFU
VDOLQLW\ ± Å 3HWU\DVKRY GRUVDO ,RQJWKDs $QDFLWHKFGLuHUHG IURP
EDVLQ DW WHPSHUDWXUHV ± ƒ&±SHFLBeRaDRVG ,VDORLQRW\LQFGXGH LWV G
Å RYHU PXGG\ ERWWRP RFFDWKHQGLDQ\RMWKSWZHVHGRFNQRRZ \HW LWV
VDQG FOD\ RU URFNV 3HWU\DVKRY. caecaE>³LQ IU2PQWYRUWKVH JDVWULF J
VSHFLHV ZLWK SK\WRSKDJRXV WHQGHQFLHV DQGUXWKHUDQVZDGHBUHV
'H -RQJ 0eRaUHDX 5HODWLYHO\ XQVBEVKHGDQWRPHZKDW ORZ D OLWWOH
LQGLYLGXDOV +DHUJUHDYHV GLVWLQFW SURWXEHUDQFH ZLWK RQH W
S @
Remarks :LOOHPRHV 6XKP LQ WKH 7DWWHUUR &OUO YRFQRQ¿UHG WK
6LHEROG ZULWWChaDenBeQESRUDUyL GHG6. sdyphoSHQGistinguenda DQG SURSRVHG WR U
VKRUW GHVPetaOophthalmusRQmigeP :LOOHPRHUVLJLQDO.nermisPEVWBSyphoIURP VXE
6XKP FROOHFWHG IURP WKH$QWDUSFWBSuSZDOVRJHWQ,WDDQGGWingueda 7KH QDPH
DQPGinermis FROOHFWHG WKH VDPH BHSyphoPsuZRVRJHWQ,WDDQGGV RQO\ IRU WK
LQ VRXWKHUQ ,QGLDQ 2FHDQ DQG DQG $UFWLF6RXWKHUQ2FHDQ +H DOVR
%RWK VSHFLHV KDG YHU\ SHFXOLBDuHrmisHWXQRWGBRXWaWRODDU RWKHU7KLV
P\VLGV 6LPXOWDQHRXVO\ KH VHZDW DGHHWUDGHHVGFUDFHRGXBEMansaDWPKT XLV
SURSHU GHVFULSWLRQ RI 2 6 7DWWHUVDOO
/LQQHDQ 6RFLHW\ RI /RQGRQ ZKLBSyphoSRKHHGDU\DHWHUDZLWK WKH
:LOOHPRHV 6XKP P. inermisPDJQDWLQRQVHGLQJXLVKHG E\ PRUH TXDGUDQJ
LQ WZR PRUH UHSRUWV KH VHQWPWRJWKEO LUIFWRO RZWKH +&QYLEQDQ
6FLHQWL¿F 6WDu SXEOLVKHG SRVWKXPRXVOQ :LFKLQRGRaeaKFORVGHOVFU
D E DV KH VXGGHQO\ GLHEOLQWHRKXUVWHTXLUWKDQ XSDWH
([SHGLWLRQ 7KH QDPH LQGLFDWHGBWKHPE$VFQRFHGRQJWKHSWKHQWLKOHVS
VWUXFWXUH RI WKH PDQGLEXODUWKSHDVURKDVXDFHWRHUWKHWLFXWRFORHWKHU
Petalophthalmus DV ZHOO DV IRUPHUKH PDWKHVBRSRGV $PRQJ.nermisKHDG FWKZRUDFIWH
* 2 6DUV E SUREDEO\ XQDRZQHBLaeca ZKSDVQLVPUHFLHVWDH RQ WKH X
:LOOHPRHV 6XKP GHDOW ZLWK GHVQFUHHGGRPRGK 2LQQH GHHWDKLO QDHQG$XVWU
ZHOO LOBoxmysis SyphoPs FXUUHQWO\, DI[DIXQQLHG KDG WKH VDPH QXPEHU R
V\QRQ\P. inermis FROOHFWHG E\ WKHV1HRUZBaeca RWKWKZLVH FRQVBUXFWHG
$WODQWLF ([SHGLWLRQ +H ZDV whkrmis¿UWKHURHGRUVFHU[FHKGWWXKQLVHBRDU
UHG ERG\ FROORXU WKH WUXQFDGWLBJQRWLVQ7KH VDFKROKRUSHDUHVPRRGVO
DQG RWKHU IHDWXUHV /DWHU *Y2HZDFURVQVLGHUHJHWYKHG 6RKWKHQ DG
Challenger PDWHULDO DV ZHOO DV WKH SXRODBWeRGGVBDQG SZHFL¿J
:LOOHP|HV 6XKP EXW HDrmWeWKZHVKH LPHQV FLHDUBinermisSDWRDWWKHU ZLWK
MXGJLQJ IURP :LOOHP|HV 6XKP ¶VcyphoPsFURPWRWKQBoaZDBWKRHU DEVHQF
UHODWHG LQBoKeDmysisSLHQDRQWRQRQ\WLGD FRQVLGHUHJ WKHP
P. inermis IURP 6RXWKHUQ ,QGLDQ2FHBQWZLQVKHG WR GLVWLQJXLVK WKH W
DOWKRXJK WKH IRUPHU ZDV GHVDULEHG GHQDBaeHGWKDSQWKH OPDWHU
)LQDOO\ * 2 6DUV ZDV DEarmigeWR RHDUBHQmWKRHQ RI WKDQ WR LWV
DQG LQ D PRUH GHWDLOHG UHSRUWXEVSHFLZHRUN³Y DU1D6DLURQ´ LQ KLV FRQ
UHFRJQL]HG LW DV GHaWDPHQ\ 7KHHQmHQJRUWWKH +DQVHQ¶V WD[RQ PX
7KH IHPDOH GHVFULEHG DQG LOOXVWUDWHBRQE\,LLOOHPRZKHVFKXZV HDUO
ZDV ORVW +H DOVR QRWLFHG D VSHKRLGHVBQHXDWLRQ RI WKH
PD[LOOLSHG SURSRGXV ³JQDWKRSRG´VQG6U+VTOWHUHUQRORJ\LQ D VS
RYHUOORNHG E\ VXEVHTXHQW DXWKRUV*X2EWKDUHV ZBWXDKHD¿UVQG WK
WR VWXG\ WKH QXPEHU RI RPPDWLGD EHK
GHVFULEHG RQO\ IRU IHZ P\LG VSHFLHV QHXDO VWUXFWXUHV DQG PXV
+DQVHQ P.DmWerJHHGBHydWRs WKH GLRSWULF VWUXFWXUH 0RUH GHW
)D[RQ GHVLJQDWHG D QHZ VXEVHFLHRQVWUXFWHG DQG WKHLU SDSH
Boreomysis suhmi)D[RQ 7KHQ +DQVHQBRQWLFHG DQG WKH ODFN RI H\HSLJ
FRPSDUHG PBDSyphoSDURRQWKH 1RUWK $WODQWLF6RXWKHUQ LQ NH\V DQG GHVFUL
DQG WKH 6RXWKHUQ 2FHDQ IRXQG7HGKLuHQGRQRHYDLQ WKHPVDWGUXHDWXHWDLO
RI WKH H\HV DQG DQWHQQDO VFDQWHDUBQGFGDHQGU1REHWKWKDFHQWPDHW
VSHFLPBLGistinguenda +DQVHQ 7KHDOHVRVKBG WKH 6RXWK $PHULFDQ FRO
WKH $XVWUDOLDQ VSHFLPHQV LQ PXVGLVSRQBOW KDYXHG UDWKHU0RTXSDURHOR
WKDQ REOQJ H\HV FORVHU LQ WKKM USHRSSXHFDWWLRQWKRI 11RUWKKSHWQDQQG

Table 1 $ OLVW RI WKH JHQHUD VXEJHQHUD DQG VSHFLHV RI
LQ WKH ZRUOG IDXQD LQFOXGLQJ WKH QHZ WD[D GHVFULE

%RUHRP\VLQDH +ROW HW 7DWWHUVDOO
Boreomysis * 2 6DUV
Boreomysis (Boreomysis)* 2 6DUV
Boreomysis (Boreomysis) acuminata 6 7DWWHUVDOO
Boreomysis (Boreomysis) arctica U¡\HU
Boreomysis (Boreomysis) atlantica RXYHO
Boreomysis (Boreomysis) bispinosa 6 7DWWHUVDOO
Boreomysis (Boreomysis) brucei 0 7DWWHUVDOO
Boreomysis (Boreomysis) californica UWPDQQ
Boreomysis (Boreomysis) chelata %LUVWHLQ HW 7FKLQGRQRYD
Boreomysis (Boreomysis) curtirostris %LUVWHLQ HW 7FKLQGRQRYD
Boreomysis (Boreomysis) dubia &RLIPDQQ
Boreomysis (Boreomysis) fragilis DQVHQ
Boreomysis (Boreomysis) hansen+ROPTXLVW
Boreomysis (Boreomysis) illigi 2 6 7DWWHUVDOO
Boreomysis (Boreomysis) incisa RXYHO
Boreomysis (Boreomysis) inopinata S QRY
Boreomysis (Boreomysis) intermedia L
Boreomysis (Boreomysis) jacobi ROPTXLVW
Boreomysis (Boreomysis) latipes %LUVWHLQ HW 7FKLQGRQRYD
Boreomysis (Boreomysis) longispina %LUVWHLQ HW 7FKLQGRQRYD
Boreomysis (Boreomysis) macrophthalma %LUVWHLQ HW 7FKLQGRQRYD
Boreomysis (Boreomysis) microps 2 6DUV
Boreomysis (Boreomysis) nobilis 2 6DUV
Boreomysis (Boreomysis) obtusata 2 6DUV
Boreomysis (Boreomysis) oparva DOW]PDQ HW %RZPDQ
Boreomysis (Boreomysis) pearcyi XUDQR HW .U\JHU
Boreomysis (Boreomysis) plebeja DQVHQ
Boreomysis (Boreomysis) rostrata OOLJ
Boreomysis (Boreomysis) semicoeca DQVHQ
Boreomysis (Boreomysis) sibogae DQVHQ
Boreomysis (Boreomysis) sphaeropsL
Boreomysis (Boreomysis) tanakai L
Boreomysis (Boreomysis) tattersalli 2 6 7DWWHUVDOO
Boreomysis (Boreomysis) tridens 2 6DUV
%RUHRP\VLV %RUHR=LW\PEHUYDQKRHüHQL
Boreomysis (Boreomysis) verrucosa 0 7DWWHUVDOO
Boreomysis (Petryashovia) VXEJHQ QRY
Boreomysis (Petryashovia) insolita 6 7DWWHUVDOO
Boreomysis (Petryashovia) kistnae LOODL
Boreomysis (Petryashovia) megalops 2 6DUV
Boreomysis (Petryashovia) urospina S QRY
Neobirsteiniamysis + HQGULFN[HW 7FKLQGRQRYD
Neobirsteiniamysis caeca %LUVWHLQ HW 7FKLQGRQRYD
Neobirsteiniamysis inermis :LOOHPRHV 6XKP

ZHUH PLQLPDO 7FKLQGRQRYD B. PHQWDLQJQWKH³QHPRVH´GDIWHU WKH
scyphops IURP WKH V\QRQ\P\ VXJJHVWLQJWKDJWDWDFKDEQLSWRSDHUSHFLPH
VSHFLHV FRXOG HTXDOO\ EH FRQVLGHUHG LQWRWKHU &RZLHGHVUFHDG
YDULDEOH VSHFLHV RU D VLEOLQJVSHFLHV RI QXRQG KLDQYHGWURHEHQGWH
KHPLVSKHUHV ,Q WKH DEVHQFHRIIDGGLWLRQDO PDWHULDOZHDUHUVKWHK
ZDV QRW UHDG\ WR PDNH ¿QDO FRQFLVLRQV SURSRVHDFRQZLRQDO
7FKLQGRQRYD DOVR FRUUHFWHG&RHH +ODRUVVLHUU %DLQGVWHKXV
7FKLQGRQRYD PBVscyphopsWS UFDLFORQ RBoreomysiWikerris peruana L V D
DB. inermis 6KH DOVR PHQWLRQBG QRQH Q XSXPHFLHV
inermis ochotsckii 7FKLQGRQRYD ZLWKHRXWSUURYLGLQJ H[SOLFLWO\ QRV
D GHVFULSWLRQ 7KLV ZDV ¿UVWUQRZDHG QERWWKBQWHBE LERXWWZLKW
=RRORJLFDO 6RFLHW\ RI /RQGRQPLVVBscDDGsDWKcyphopsD+HH ZDVWDO VR SU
EH FRQVLGHUHG QRPHQ QXGXP XQDZBirsteRamysis GHVLJQDWHG ERU
% FHVFX VXJJHVWHG WKDW 7FHKULXQ 'HVLJ
&KLOH 7UHQFK ³SRVVLEO\ EHORQJLQJ XSRnerRmisBScyphopsDB.caeca 7SKLFLGHV
B. inermis peruana +H SURYLGHG VRPH FKDUDFWHUVRQDOQXHG WUHDWLQJ